Microstructural and emission properties induced by Na incorporation in pure sulphide CIGS absorber

Richel Dongmo, Rémi Demoulin, Nicolas Barreau, Léo Choubrac, Fabien Pineau, Etienne Talbot, Sébastien Duguay

▶ **To cite this version:**

Richel Dongmo, Rémi Demoulin, Nicolas Barreau, Léo Choubrac, Fabien Pineau, et al.. Microstructural and emission properties induced by Na incorporation in pure sulphide CIGS absorber. Journal of Alloys and Compounds, inPress, 1037, pp.182582. ⟨10.1016/j.jallcom.2025.182582⟩. ⟨hal-05221794⟩

HAL Id: hal-05221794

https://hal.science/hal-05221794v1

Submitted on 25 Aug 2025

HAL is a multi-disciplinary open access archive for the deposit and dissemination of scientific research documents, whether they are published or not. The documents may come from teaching and research institutions in France or abroad, or from public or private research centers.

L'archive ouverte pluridisciplinaire **HAL**, est destinée au dépôt et à la diffusion de documents scientifiques de niveau recherche, publiés ou non, émanant des établissements d'enseignement et de recherche français ou étrangers, des laboratoires publics ou privés.

HAL Authorization

Microstructural and emission properties induced by Na incorporation in pure sulphide CIGS absorber

Richel Dongmo[1], Rémi Demoulin[1]*, Nicolas Barreau[2], Léo Choubrac[2], Fabien Pineau[2] Etienne Talbot[1], Sébastien Duguay [1]

[1] Univ Rouen Normandie, INSA Rouen Normandie, CNRS, Normandie Univ, GPM UMR 6634, F-76000 Rouen, France

[2] Nantes Université, CNRS, Institut des Matériaux de Nantes Jean Rouxel, IMN, F-44000 Nantes, France

*Corresponding author; Email: remi.demoulin1@univ-rouen.fr

Abstract

Pure sulphide chalcopyrite $Cu(In,Ga)S_2$, referred to as CIGSu, is a promising material for the use as top cell in tandem photovoltaic applications. This report aims at investigating the influence of Na incorporation on the optical and structural properties of the CIGSu. Na treatments are indeed known to largely improve the performances of the selenide chalcopyrite $Cu(In,Ga)Se_2$, leading to record efficiencies amongst the thin film technology. In this work, CIGSu layers subjected to different Na incorporation strategies were grown on Mo or ITO rear contact. The crystalline quality of the CIGSu layers was investigated by XRD diffraction showing a homogeneous phase of CIGSu. On the other hand, optical properties of CIGSu were carried out by cathodoluminescence spectroscopy. The analyses demonstrate the passivation of the CIGSu layer induced by Na incorporation. Also, the formation of an in-depth band grading inside the CIGSu layer was evidenced and linked to the Na incorporation. Moreover, atom probe tomography revealed a planar segregation of Na along the grain boundary, evidencing the diffusion of Na through the ITO rear contact.

Introduction

Silicon solar cell technology currently dominates the photovoltaic (PV) market, representing more than 90% of the global production [1]. The remaining part is mostly occupied by thin film technology. In the latter, polycrystalline $Cu(In,Ga)Se_2$ cells (referred to as CIGSe) are amongst the most efficient, having achieved in 2024 a record efficiency of 23.6% [2]. Despite its high efficiency, the development of CIGSe, and mono-junction solar cells in general, are approaching the Shockley-Queisser (SQ) limit (η_{SQ} = 32.2 %) [3], reducing their potential for future progress. To overcome this limit, III-V multi-junction solar cells have been designed, reaching in 2020 a record efficiency of 47.1% [4]. Nevertheless, large-scale development of III-V multi-junction solar cells is limited by their manufacturing costs. Since the early 2010s, tandem structures combining c-Si and thin film technologies has gained interest. Theoretical calculations evidenced that an efficiency of more than 45% could be reached by positioning a 1.7 eV band gap cell above a 1 eV top cell [5]. The silicon technology is the most mature technology for the bottom cell due to its adequate band gap of 1.1 eV and its high efficiency (reaching more than 26% [6]). Concerning the top cell, device based on pure sulphide chalcopyrite $Cu(In,Ga)S_2$ (also referred to as CIGSu) is an interesting candidate due to its wide band gap, high performance [7] and long-term stability [8,9]. The present study focuses on the investigation of CIGSu as polycrystalline thin film, material that has been much less studied than its selenide counterpart. This lack of investigations is assuredly one of the reasons for the lower progress in the performance achieved by the related devices. Recent studies have shown that the chalcopyrite phase is much less tolerant to copper deficiency than the

selenides [7,10]. This latter implies that the CIGSu films has to be very close to stoichiometry to remain single phase. As mentioned in [10], such a poor tolerance to copper off-stoichiometry questions about the role played by sodium doping on both the crystalline phase formed and the density of compensating point defects.

Regarding CIGSe based solar cells, the efficiency boosts achieved during both 1990s and 2010s are linked to Na and heavy-alkali doping, respectively [11]. Na doping is known to minimize the density of compensating defects and to passivate grain boundaries [12–16]. The incorporation of Na into chalcopyrite films can be performed following diverse approaches, namely (i) either before the deposition of the absorber through the deposition of a thin sodium-containing layer, (ii) during the deposition by supplying sodium-containing compound (DDT: during deposition treatment), or (iii) after CIGS completion by treating it with sodium-containing compound (PDT: post deposition treatment). It should be noted that glass substrates containing Na (e.g. soda lime glass or SLG) can also be used as the Na source since alkali species are able to diffuse throughout polycrystalline Mo rear contact, as shown in the case of CIGSe [17]. Recently, Choubrac *et al.* showed that the combination of DDT and PDT was crucial to increase and stabilize the open circuit voltage (V_{oc}), the fill factor and thus the power conversion efficiency of the CIGSu based cell when using SLG/Mo rear contact [18]. Nevertheless, if one targets tandem 4T application, the use of Mo rear contact is banned because of its opacity and should thus be replaced by a transparent contact. ITO (In_2O_3:Sn), which combines conductivity and transparency in the visible spectrum, was successfully used as rear contact for both CIGSe cell [19–21]. ITO was chosen because it can sustain the relatively high temperature needed for absorber growth and does not decompose in basic media such as those used for chemically deposited CdS and ZnOS buffers layers. However, the permeability of ITO to Na species needs to be clarified as some studies reported that depending on growth conditions ITO can slow down the Na diffusion or act as a diffusion barrier [13,20,21].

The goal of the present work is to investigate the influence of Na doping on the chemical and optoelectronic properties of CIGSu polycrystalline thin films by means of X-Ray diffraction, electron backscatter diffraction, cathodoluminescence and atom probe tomography. As detailed below, films grown on either SLG/Mo or SLG/ITO are studied with and without intentional additional Na doping.

Experimental methods

Films preparation

600-nm-thick CIGSu layers were deposited on 1-mm thick soda lime glass (SLG) substrate coated by either 400 nm-thick Mo (DC-Sputtered) or 400 nm-thick ITO (provided by SOLEMS company). The CIGSu films were synthesised by co-evaporation following the 3-stage process in a dedicated vacuum chamber [22,23]. The first stage was performed at substrate temperature of 300°C, whereas second and third stages at 580°C. Details on the 3-stage process are presented on Figure S1. As summarized in the Table 1, four kinds of samples have been produced. A1 and A2 were deposited on SLG/Mo substrates, whereas A3 and A4 were deposited on SLG/ITO substrates. Both A1 and A3 underwent Na doping through NaF supply during the third stage (i.e. DDT) and as post-deposition treatment (i.e. PDT). A2 and A4 films did not undergo intentional Na-doping, only Na diffusing from the substrate could dope the films; this process is referenced to as diffusion throughout the contact (i.e. DTC). The figure 1 schemes the structures of the samples and the possible origins of Na contained within the investigated CIGSu films.

Structural and chemical characterizations

All SLG/contact/CIGSu were investigated by XRD to evaluate their crystalline properties. These experiments were performed using a (θ - 2θ) Malvern empyrean diffractometer. The exciting source is made of a monochromatic Co radiation with a wavelength of λ=1.7889Å. The obtained data have then been converted into Cuα (λ=1.5406 Å) XRD data as it is the most common source in the literature. EBSD contrast images were obtained using Oxford EBSD software *in situ* in a PFIB (Plasma Field Ion-Beam) Helios G4 CXe Thermo scientific. The sample was tilted at 70° and the analysis was performed using an electron beam with a voltage of 20 kV and a current of 1.6 nA. For the local analysis, 10° bevelled surfaces have been prepared using PFIB. The preparation process has been performed as

follows: (i) 3 µm thick of platinum (Pt) layer was deposited to protect the surface, (ii) the surface was tilted to form an angle of 10° with the ion beam, (iii) a milling at (30 kV, 4 nA) was performed followed by a cleaning step at (2 kV, 2 nA) to remove the damage caused by the high voltage/current milling.

APT was used to investigate the Na distribution inside the CIGSu layer. The APT analysis is based on the field evaporation effect produced on surface atoms in tip-shaped samples. First, the sample has to be prepared in the shape of nanometric tip by conventional lift-out and annular milling methods [24]. The lift-out procedure was carried out at 30 kV followed by a cleaning step at 2 kV to remove the damaged surface, due to Xe ions from the PFIB beam, and reach a curvature radius of around 50 nm. The analysis has then been performed using a Laser-Assisted Wide-Angle Tomographic Atom Probe (LAWATAP), using a femtosecond UV pulsed lased (350 fs, 100 kHz, 343 nm) with a laser pulse energy of 1.2 nJ and a detector yield of 0.62. Analyses have been performed in a vacuum chamber (10^{-10} mbar), at a temperature of 30K. The 3D reconstruction was carried out using the home-built GPM3Dsoft software.

In order to study the local optoelectronic properties of the CIGSu, CL measurements were carried out at room temperature using a HORIBA-HCLUE setup, *in situ* in a JEOL JSM-M7900F scanning electron microscope. The light emitted after excitation of the sample by the electron beam was collected and directed toward an IHR 320 (320 mm focal length) spectrometers using a paracolic mirror. The signal was then detected by a Jobin-Yvon CCD camera which operates on a UV-Visible range (200 to 1200 nm window). A 600 lines/mm grating (blazed at 500 nm) monochromator was chosen for the spectrum acquisition. The acceleration voltage of the electron beam was set at 10 kV with an electron beam current of 440 pA. The spectrum acquisitions were realized in scanning mode at the surface of the sample for a duration of 2 seconds. Map acquisitions were performed in hyperspectral mode using a 150 lines/mm grating (blazed at 500 nm) within the objective of collecting the maximum signal. The voltage and current of the electron beam were set at 5 kV and 4 nA respectively. The previous analysis conditions were obtained by calculating the electron trajectory within the samples using of CASINO software [25,26]. The CASINO simulations are detailed in the supplementary materials on Figure S2. The results obtained are based on Monte Carlo electron energy loss simulation. The Kanaya-Okayama has been chosen as simulation model [27].

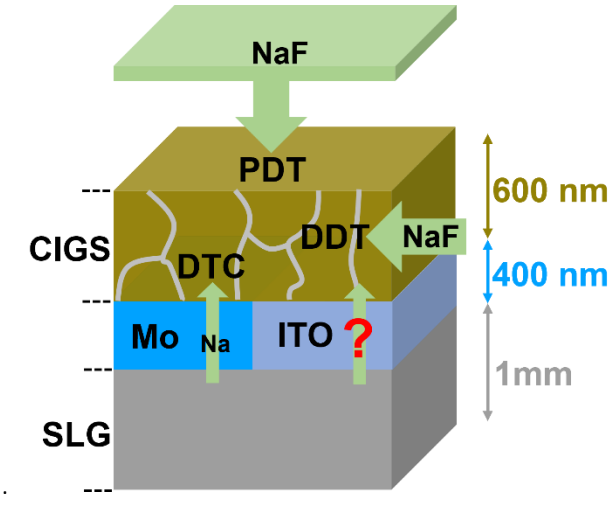

Figure 1: Schematic representation of the structure of CIGSu samples showing related incorporation strategies. The question mark on the ITO side refers to the fact that so far, we cannot conclude on the permeability of ITO to Na-compounds from the glass.

Table 1: Description of the Na incorporation strategies used for the samples A1 to A4:

Samples / Na incorporation Strategies	A1	A2	A3	A4
Rear contact associated	Mo	Mo	ITO	ITO
DTC	YES	YES	?	?
DDT + PDT	YES	X	YES	X

Results

In order to study the crystallographic properties of CIGSu layers and state on the eventual presence of secondary phases, XRD measurements have been performed on the 4 samples of this study. Figure 2.a shows the diffraction patterns of all 4 samples. The diffractograms of samples A1 and A2 display Cu(Ga,In)S_2 and Mo related peaks only. The main CIGSu peak is observed at 28° and corresponds to the (112) reflexion. The remaining CIGSu peaks are observed at 57.8°, 55.2°, 46.5, 32.5 and 18° and are attributed to (224), (312/116), (220/204), (200/004), (101) reflexions, respectively, as detailed in (JCPDS # 32-0339). Additionally, the diffractograms of A1 and A2 show a peak at 40.5°, which corresponds to Mo (110) reflexion (JCPDS # 01-1208). A3 and A4 show the same CIGSu peaks as A1 and A2. The difference is related to the presence of ITO (rear contact in A3 and A4) peaks observed at 51°, 35.4°, 30.5° and 21.5° attributed to (440), (400), (222) and (211) reflexions respectively (JCPDS # 060416). Although the CIGSu (101) reflexion signal is very weak on A3 and A4, it still appears in both cases as shown on Figure 2.b. The presence of this peak on all samples confirms the chalcopyrite nature (space group $\bar{I}42d$) of the CIGSu absorber. Since the most intense CIGSu peak, corresponding to the (112) reflexion, does not split into two contributions, it can be confirmed that a single crystalline CIGSu phase has been obtained [28]. This is likely due to the high-quality of the growth process. In the meantime, Na incorporation does not seem to have much influence on the crystalline quality of CIGSu. Indeed, samples with the same rear contact show a similar diffraction pattern. In CIGSu absorber, the GGI can be directly calculated from the position of the (112) using the following equation derived from the Vegard law [29,30]:

$$y = (1 - GGI) * CIS(2\theta) + GGI * CGS(2\theta) \qquad (1)$$

where y is the 2θ angle of the (112) reflexion of the analysed samples. CIS(2θ), 27.89° (JCPDS # 85–1575) and CGS(2θ), 29.1° (JCPDS # 75-0103) are the 2θ angles of the (112) peak measured on $CuInS_2$ and $CuGaS_2$ compounds respectively. In these samples, the GGI has been estimated at 0.09 ± 0.02. Then, the composition of the absorber can be noted $CuIn_{0.91}Ga_{0.09}S_2$.

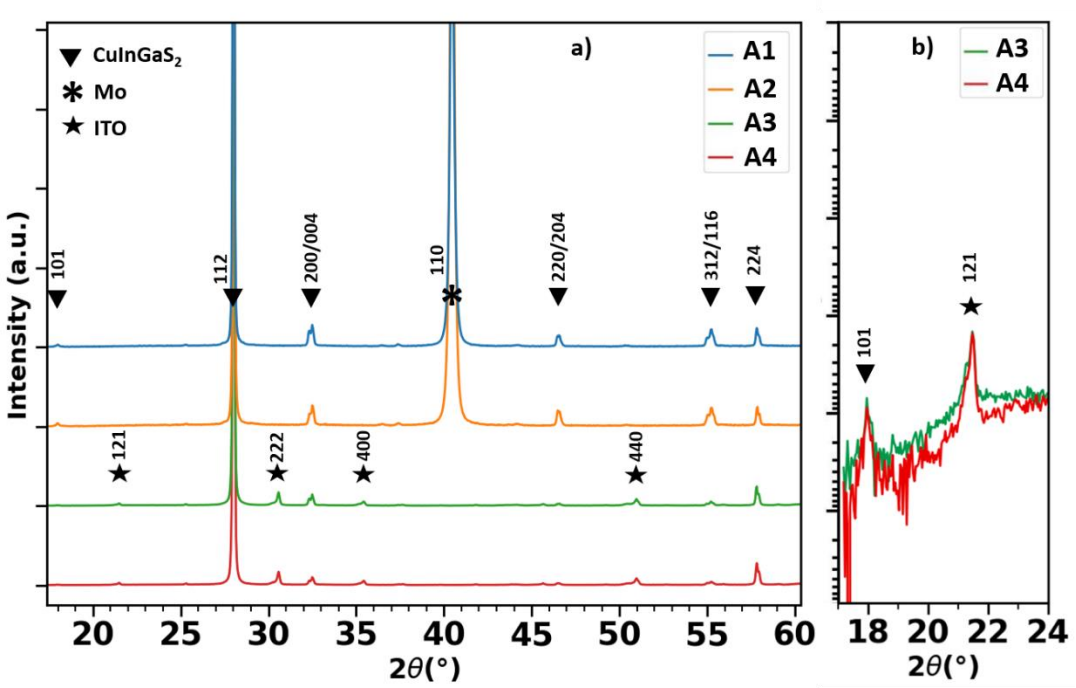

Figure 2: a) XRD spectra of all CIGSu thin films A1 to A4. b) Magnification of XRD pattern of A3 and A4 samples, in logarithmic scale, highlighting the presence of the CIGSu (101) reflexion at 18°.

Figure 3 shows a typical CL spectrum collected on sample A2. The CL experiment has been performed using a 10 kV electron beam in order to probe the whole CIGSu absorber (Figure S2). This spectrum is characterized by two emission peaks. The most intense peak centred at 1.6 eV can be attributed to the band-to-band emission of the CIGSu absorber. Thereafter, the position of the maximum intensity of this peak has been considered as the bandgap (E_G) of the material. The small and broad peak observed around 1.35 eV may correspond to a defect emission. Figure 4.a displays the resulting normalized CL spectra of samples A1 and A2 collected in the same conditions. In A1, the band-to-band emission of CIGSu (E_G = 1.59 eV) is shifted toward lower energies compared to A2 (E_G = 1.60 eV). Moreover, the intensity of the defect band observed on sample A2 at 1.35 eV is significantly reduced on A1. Similar defects have already been observed around 1.35 eV in the literature, and have been attributed to Cu_{III} antisite [31].

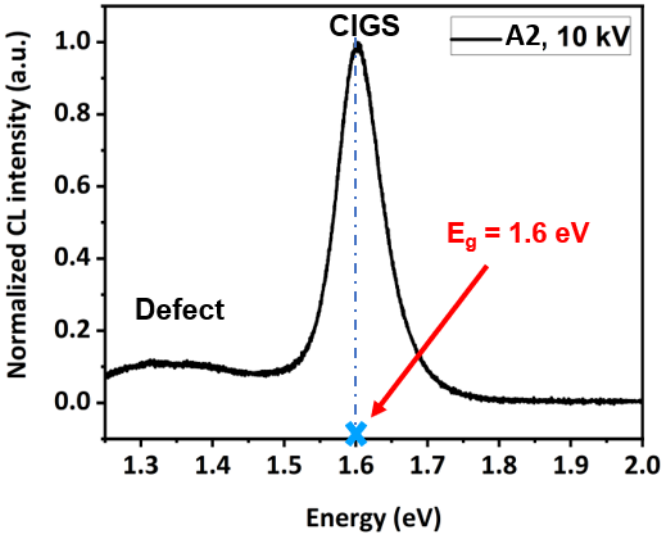

Figure 3: CL spectrum of sample A2 collected at 10 kV in scanning mode on a surface of 50 × 50 µm^2.

Similarly, Figure 4.b shows the A3 and A4 normalized CL spectra. In the case of ITO rear contact, no differences are highlighted concerning the position of the band-to-band emission peak of CIGSu, which is estimated at E_G=1.59 eV in both cases. Again, a defect band characterized by the presence of a less intense emission broad band, at around 1.45 eV, has been observed on A4 but looks to be significantly reduced on A3. Depending on the rear contact (Mo for A1 and A2 or ITO for A3 and A4), the defect band is observed at different energies. That might suggest the existence of two different kind of defects as function of the nature of the rear contact. In fact, the defect present in A4, evidenced on CL spectrum as a broad band around 1.40 to 1.45 eV, might be related to the formation of Cu vacancies V_{Cu} and Cu_{In} anti-site, as described in pure $CuInS_2$ absorbers in the literature [10]. However, in spite of the different nature of the rear contact and maybe of the defects in the CIGSu layer, application of alkali treatments seems to be beneficial to the layer properties. In A1 and A3, which both underwent Na DDT and PDT, no defects band are observed. This confirms the efficiency of such treatments in passivating the defects, as usually observed in CIGSe [32].

It has been shown in CIGSe that the bandgap energy can be directly linked to the GGI ratio of the absorber [33]. Here, the calculation has been adapted for CIGSu. The energy of the band-to-band emission of CIGSu extracted from CL spectrum has been used to estimate the GGI following the equation 2:

$$E_G(x) = (1-x) * E_G(CIS) + x * E_G(CGS) - b * x(1-x) \qquad (2)$$

Where x is the GGI, $E_G(x)$ the band gap of the $Cu(In,Ga)S_2$ layer measured by CL. E_G(CIS) and E_G(CGS) represent the band gap values of $CuInS_2$ (1.54 eV) [34] and $CuGaS_2$ (2.43 eV) [35] alloys respectively. b is the optical bowing coefficient and has been chosen equal to 0.2 [36]. The GGI ratio was calculated to be equal to 0.087 ± 0.003 and 0.090 ± 0.003 respective band gaps of 1.59 eV (for A1, A3 and A4) and 1.60 eV (for A2). This result is in accordance with the value of the GGI measured previously by XRD. The origin of the shift might be related to a slight modification of the GGI in the sample A4 and will be discussed further.

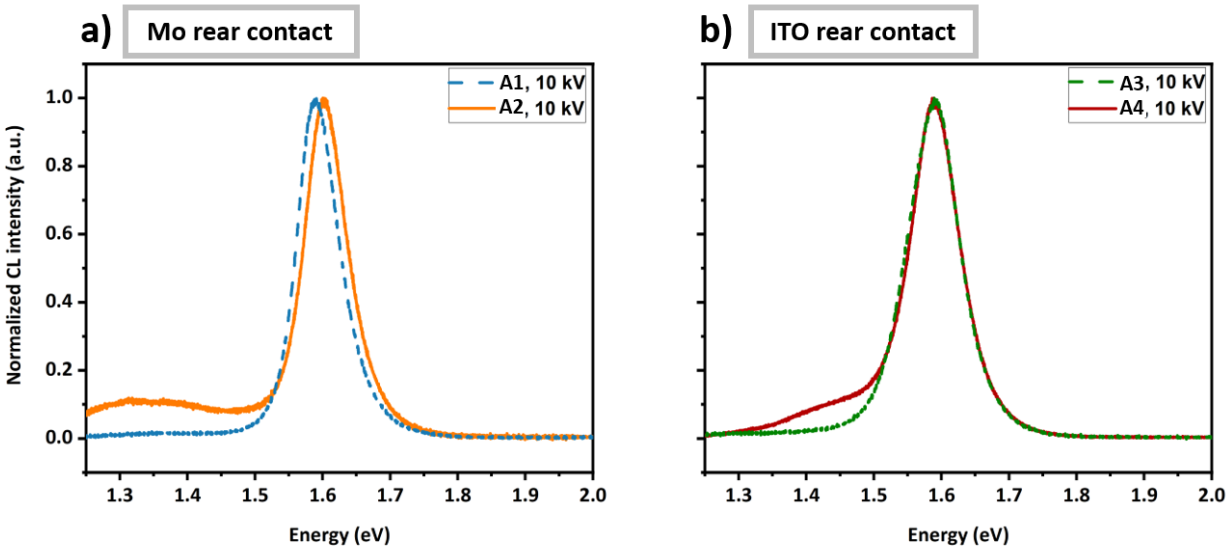

Figure 4: Normalised CL spectra collected at 10 kV in scanning mode on a surface of 50 × 50 µm^2 for (a) samples A1 and A2, and (b) samples A3 and A4.

To investigate the depth homogeneity of the CIGSu absorber, EBSD and CL experiments have been performed on bevel surfaces. Figure 5.a shows a schematic representation of a 10° bevel surface performed on the typical structure presented on Figure 1. According to CASINO simulations presented in Figure S2, the CL measurements have been

realised with 5 kV voltage and 4 nA current probe to scan the first nanometres of the bevel surface. First, an EBSD band contrast was performed in order to observe the grain distribution on the CIGSu bevelled surface. Figure 5.b represents the band contrast micrograph acquired in the bevel configuration. On the one hand, bright regions marked by the red arrows are attributed to the grain interior (GI). On the other hand, dark regions, marked by white arrows are attributed to grain boundaries (GB). Moreover, some twin boundaries, marked by yellow arrows, can be observed in some areas. This band contrast shows a strong GB density in the CIGSu layer. Figure 5.c represents the maximum CL intensity distribution of the band-to-band emission of the CIGSu peak (around 1.6 eV) along the bevel surface of sample A1. The CL intensity is clearly not homogeneously distributed all along the map. The comparison between the EBSD band contrast and the CL intensity distribution map clearly evidences that the CL emission observed in Figure 5.c originates mainly from GI. It is illustrated by the green circle marking the same grain on all maps. Darker emission lines formed inside the CIGSu layer can be attributed to the GB, which are known to be mostly non-radiative recombination centres. The lower intensity observed near the rear contact, is due to the bevel geometry resulting in a thinner CIGSu thickness probed (i.e. a lower CL signal). Figure 5.d represents the energy distribution of the CIGSu band-to-band emission along the bevel surface. Two different regions can be clearly identified, a low energy region (≈1.57-1.58 eV) in the upper part of the CIGSu layer, distributed over 200 nm from the top and a high energy region (≈1.61 eV) spread over 360 nm in the bottom part of the layer. Local spectra at different depth have been presented in Figure S3 to confirm the energy shift toward higher energy near to the rear contact. This phenomenon also known as band gap grading, has already been evidenced in CIGSe layer and is known to arise from the rearrangement of In and Ga in the absorber depth [39]. It has been demonstrated that such band grading allows to improve the carrier collection, the open-circuit voltage and the fill factor in CIGSe layer [37]. Unlike CL intensity, the energy mapping of the CIGSu peak does not show a particular difference in emission between the grain and the grain boundary. This might be because the signal resulting from the grain boundary is overshadowed by the grain interior signal due to the small width of the grain boundary compared to the grain interior.

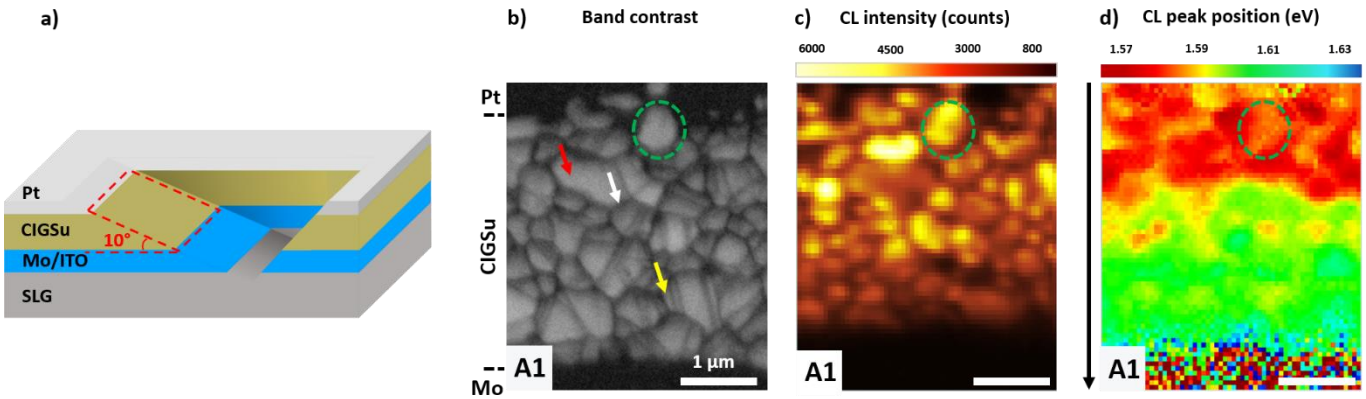

Figure 5: (a) Schematic representation of a 10° bevel cross section of Pt/CIGSu/(Mo or ITO)/SLG, the red dashed rectangle represents the investigated area in b, c and d. (b) EBSD band contrast micrograph of the bevel of the sample A1, (c) corresponding CL intensity map of A1 and (d) CL energy distribution map of the CIGSu peak. The scale bar corresponds to 1 µm.

Built on the same approach, Figures 6.a-c represent the maximum CL intensity distribution of the CIGSu peak for A2, A3 and A4 respectively, collected on bevel surfaces. The dark region observed on the top of each layer corresponds to the Pt protective layer deposited on the CIGSu layer during the bevel preparation. No significant difference is observed from one sample to another in term of CL intensity. As in the case of A1, the CIGSu CL intensity is predominant in the grain interior and tend to decrease at the grain boundaries for all sample. This observation evidences significant losses due to the presence of non-radiative recombination centres near the grain boundaries.

Also, the CL intensity does not depend on the grain size and appear to be heterogeneously distributed from one grain to another.

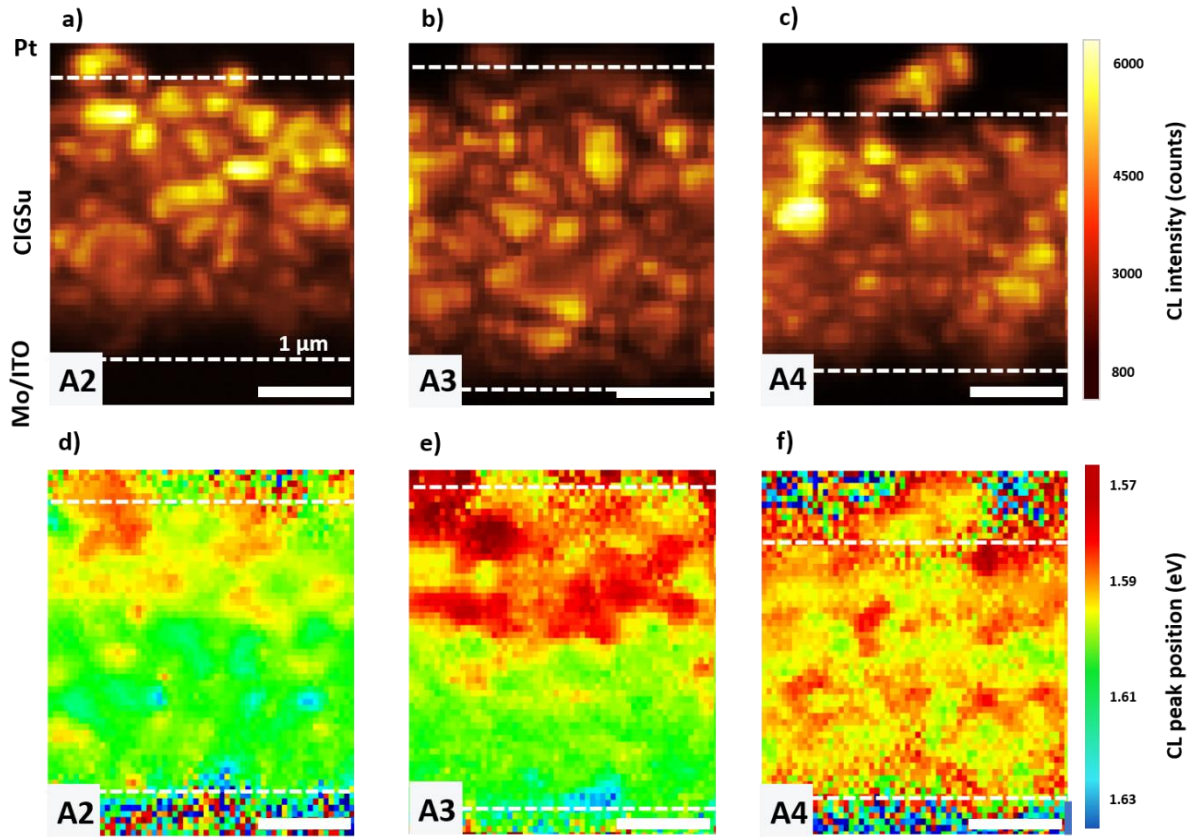

Figure 6: (a-c) CL intensity map and (d-f) CL energy distribution map of the CIGSu peak for A2, A3 and A4 collected on a bevel surface. The scale bar is the same for every map and is equal to 1 µm. The dark region at the top of each intensity map corresponds to the areas covered by the protective Pt layer. White dotted circles surround potential traps in the CIGSu.

Figures 6.d-f show the energy distribution of the band-to-band emission of the CIGSu layer with respect to its depth for A2, A3 and A4, respectively. For both samples which underwent Na PDT and DDT, A1 and A3, the evolution in terms of energy distribution seems to be quite similar independently of the rear contact. In fact, sample A3 presents the same characteristics as observed in sample A1, showing two clearly defined parts, with lower energies at the surface (around 1.58 eV) and higher energies near the rear contact (around 1.61 eV). Concerning the sample A2, if the lower part of the sample is dominated by higher energies, as observed in A1 and A3, the upper part evidenced more heterogeneities with energies ranging from 1.58 eV to 1.60 eV. Finally, the sample A4 shows only one heterogeneous region in the layer depth, with energies ranging from 1.58 eV to 1.61 eV.

In order to explain the evolution of the band-to-band energy in the depth of the CIGSu layer, averaged profiles have been computed on all four energy maps and are displayed in Figure 7. Each curve represents the evolution of the band gap energy averaged on the energy map width along the depth of the CIGSu layer (in the direction of the black arrow represented in Figure 5.c). It must be noted that in each profile, the first measurement point may be altered due to the roughness of the sample surface, inducing lower CL signal and higher noise. The two black curves (stars and circles) correspond to CIGSu layers deposited on a Mo rear contact (A1 and A2). The energy variations amplitude observed in A1 (≈ 25 meV) is larger than the one observed in A2 (≈ 15 meV). Moreover, their respective profiles evidenced that the energy measured in A2 is higher than in A1, all along the depth of the CIGSu layer. This observation

confirms the energy shift toward higher energies previously observed on CL spectra (figure 4.a). By comparing these energy profiles with the CL spectra acquired on the sample surface (Figure 4), it can be assumed that the position of the peak in the CL analysis of the sample surface may represent the minimum of the band gap in the film depth. Concerning their shape, in A1 profile, a two-step evolution can be identified. The first step corresponds to a slight energy decrease along the first 200 nm. The second step shows a significant increase of energy toward the CIGSu/Mo interface. Such bandgap evolution can be defined as a double grading bandgap and is usually beneficial for the cell performances by improving the charge collection at the contact [38]. For A2, the energy tends to increase all along the depth, from the top to the bottom of the CIGSu layer. However, a slight bump can be observed on the average energy curve, which might be induced by the presence of localised areas of higher energy in the middle of the layer (highlighted by white dotted circle in figure 6.d). These localised areas are potential energy barrier, trapping electrons and therefore, causing Shockley-Read-Hall recombination [39]. This phenomenon is known to degrade the properties of the solar cell. Comparing A1 and A2, it appears clearly that the formation of the double band-grading, observed in A1, is favoured by the application of Na PDT and DDT. In fact, it has been shown that Na doping in CIGSe induces interdiffusion between In and Ga atoms, modifying the GGI, and so the bandgap, along the CIGSe depth [40]. Such process seems to be similar in CIGSu layers.

Between samples A3 and A4 grown on ITO rear contact (red curves), the observations are different. In A3, which underwent Na PDT and DDT, the averaged energy profile follows the same evolution as observed in A1, with similar amplitude. This evidences that the band grading triggered by Na PDT and DDT must be independent of the nature of the rear contact. On its side, A4 exhibits a quite different shape, with a quasi-flat energy profile, characterised by an energy variation of only 4 meV from 150 nm up to the ITO contact. Without Na treatments, two main differences can be observed by comparing A2 and A4. The first concerns the absence of a bandgap increase in the depth of the sample A4. As no Na PDT neither DDT have been applied on both samples, this difference may be linked to the diffusion of Na from the SLG substrate trough the rear contact. In fact, if Na doping induces a variation of the GGI in the layer [40], the absence of bandgap variation in the depth of the sample A4 might evidence a higher diffusion rate of Na atoms through the Mo contact than ITO contact. The second difference concerns the shift in the lower energy observed in the sample A4. As the bandgap can be directly linked to the GGI ratio along the sample depth, this indicates the presence of a lower amount of Ga in the CIGSu layer. This may be induced by the diffusion of Ga atoms to form a Ga oxide at the CIGSu/ITO, as already highlighted in the case of CIGSe [20].

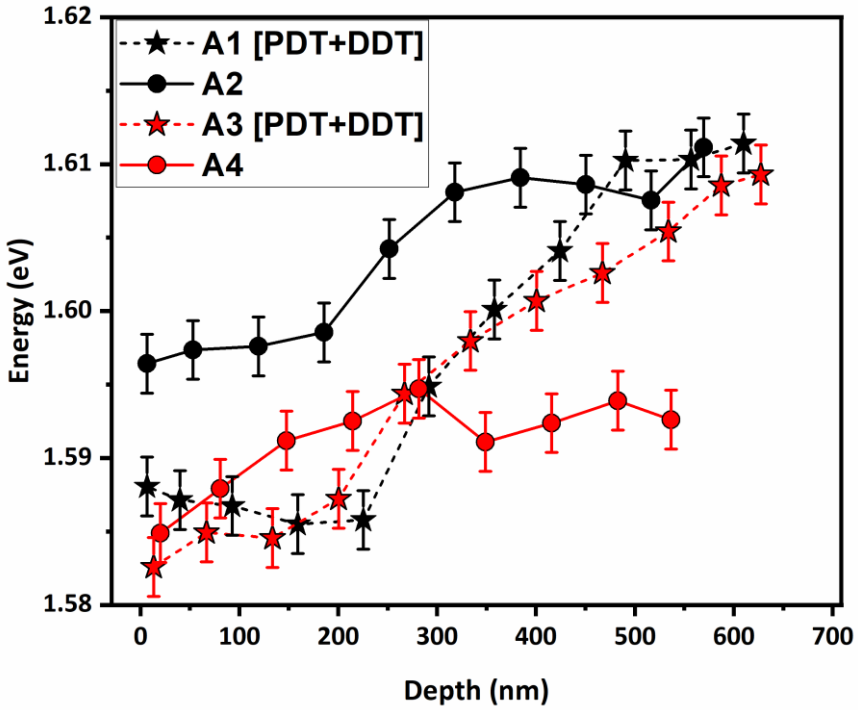

Figure 7: Averaged bandgap profile of all four samples extracted from energy distribution maps. Zero position corresponds to the surface of the sample. Black and red curves correspond to the CIGSu layer grown on Mo and ITO rear contact, respectively.

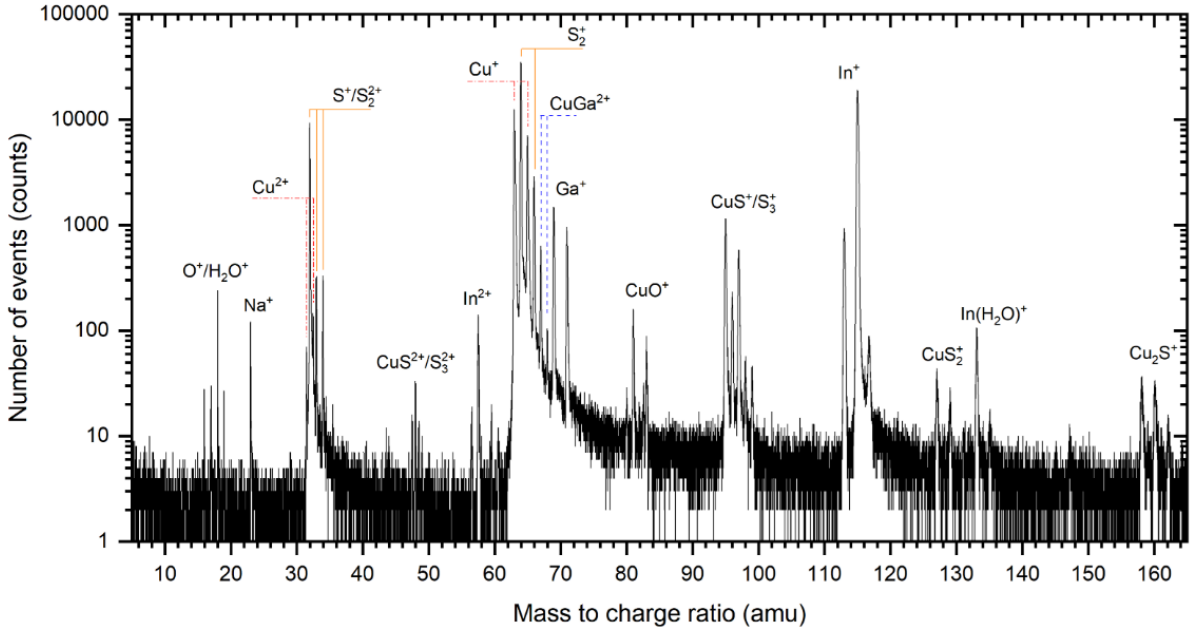

Figure 8: Atom probe mass spectrum of a CIGSu layer deposited on ITO rear contact (sample A4).

A chemical characterisation of the sample A4 has been performed using APT in order to evaluate the presence of Na in the CIGSu layer. The atom probe mass spectrum is presented in the Figure 8. The later presents the chemical species detected during the evaporation. Cu, In and Ga are detected as single ions Cu^+, Cu^{2+}, In^+, In^{2+} and Ga^+ respectively. Sulphur is mainly detected as molecular ions in the form of S_2^+, S_2^{2+}, S_3^+ and S_3^{2+}. Moreover, Cu, Ga and S are also detected as molecular ions CuS^+, CuS^{2+}, $CuGa^{2+}$, CuS_2^+ and Cu_2S^+. It can be noted that the detection of O^+, H_2O^+, CuO^+ as well as $In(H_2O)^+$ may be due to the presence of O_2 and H_2O molecules in the APT analysis chamber. It is interesting to note that Na atoms are also detected as single ions Na^+. As no Na treatment has been performed on the sample A4, this observation evidenced that the Na diffuses through the ITO rear contact. As Mo, in these growth conditions, ITO seems to allow the diffusion of Na atoms from the SLG substrate. In addition, no Xe ions were detected, showing that Xe was not implanted in the structure during the FIB milling process and thus that the cleaning step was successful.

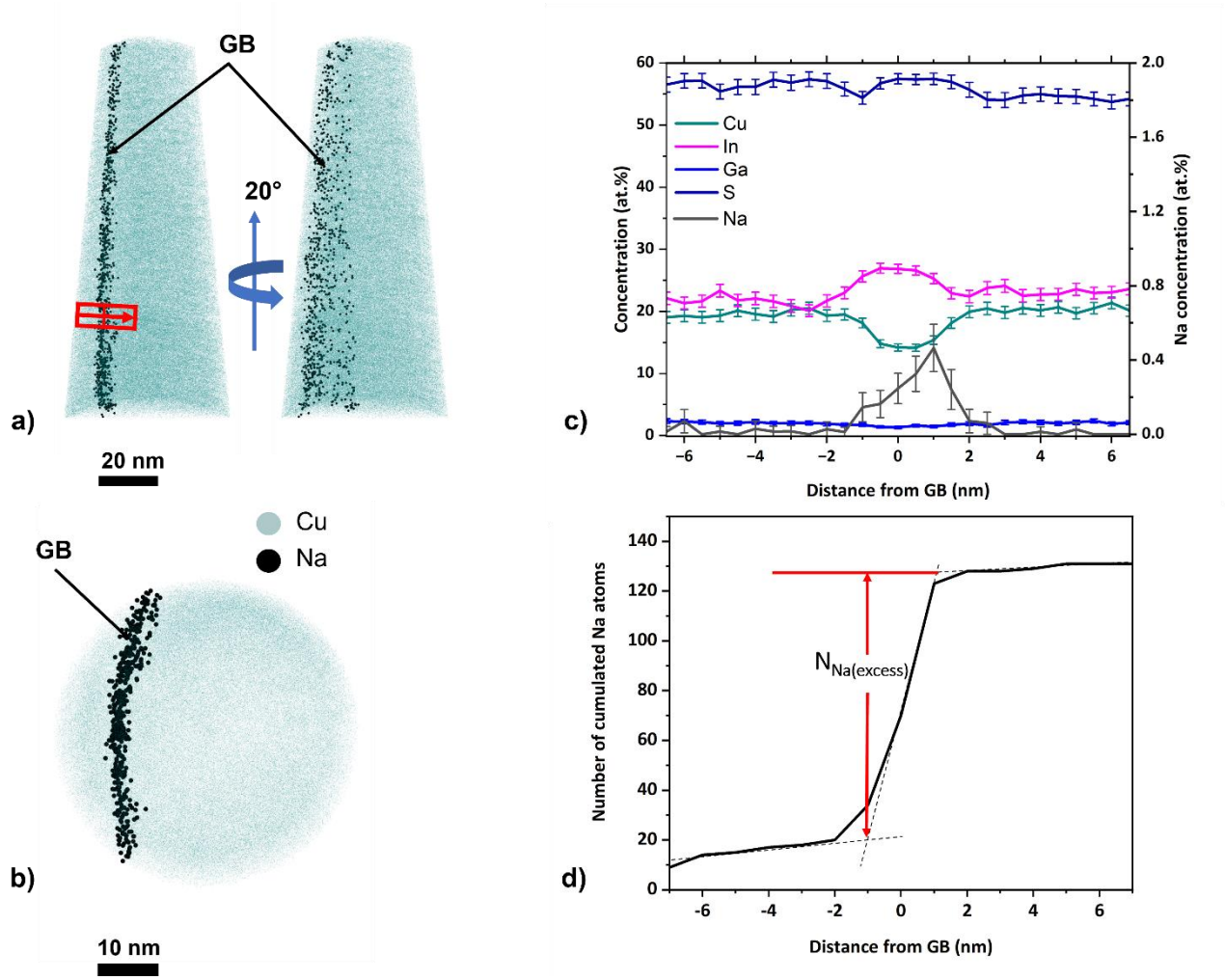

Figure 9: a) 3D reconstruction showing the Cu and Na atomic distribution around a grain boundary, in the sample A4, resulting from an atom probe tomography analysis. Na atoms size have been increased and are represented in black while Cu atoms are represented in green. b) Top view of the 3D volume showing the segregation of Na along the grain boundary. c) Concentration profile and d) cumulative density profile of Na atoms passing through the grain boundary, measured in a 20 × 10 × 13 nm^3 volume.

A 3D reconstruction of the tip-shaped sample has been performed in order to quantify and locate Na atoms. The APT sample was prepared perpendicularly to the surface. The analysed volume corresponds to the middle of the CIGSu layer. Figure 9.a and b show the 3D atomic distribution of Cu atoms (green dots) and of Na atoms (black dots). The 3D reconstruction of the CIGSu volume highlights the presence of Na atoms all along a grain boundary as observed in the literature in the case of CIGSe layers [14,15]. Moreover, low amount of Na has also been detected within the grains. The concentration has been estimated at 1.8×10^{18} at/cm^3. By comparison, APT analysis performed on sample A3 (not shown here) has evidenced a larger amount of Na inside the grains, with a concentration estimated at 3.2×10^{18} at/cm^3. The mass spectra around Na peak, of both samples, are presented in Figure S4. A composition profile, presented in figure 9.c, has been computed throughout the grain boundary in a 20 × 10 × 13 nm^3 red box shown in Figure 9.a. The composition of species in both grains is similar and can be estimated at 19 ± 1 at.% of Cu, 22 ± 1 at.% of In, 2.3 ± 0.4 at.% of Ga and 56.7 ± 2 at.% of S. Cu and S deviation from the expected stoichiometry may be induced by the important overlapping between Cu^+, S_2^+ peaks (around 60 to 66 a.m.u) on the mass spectrum. Also, Cu droplets can form at the surface of the sample during the preparation [41]. This phenomenon is known and may result in a loss of Cu in APT experiments. On the other hand, In and Ga species, seems to be detected in accurate proportions within experimental errors (In + Ga ≈ 25%). Therefore, analysis conditions were good enough to quantify the GGI ratio, estimated at 0.094 ± 0.02. This corroborates the previous values found using XRD and CL (obtained on much larger scale). At the grain boundary, the composition profile evidences In enrichment of 23 % as well as Cu depletion of 30 % while S and Ga compositions remain constant. This might represent the source of potential Cu_{In} antisite or V_{Cu} inside the CIGSu absorber. In agreement with these observations, Raguwanshi *et al.* reported that Cu-poor grain boundaries are mainly found in Ga-poor CIGSe compound [15]. Besides, the Na composition at the grain boundary is estimated at 0.4 ± 0.1 at.%. To quantify the segregation of Na atoms at the grain boundaries, the Gibbsian Interfacial excess (Γ_{Na}) can be used [42]. This parameter is defined as the number of segregated Na atoms per unit of interfacial area. The number of Na atoms segregated at the grain boundary (noted $N_{Na(excess)}$) can be directly extracted from APT data using the cumulative density profile represented in Figure 9.d. Therefore, the Gibbsian Interfacial excess can be calculated using the following equation:

$$\Gamma_{Na} = \frac{N_{Na(excess)}}{\eta A} \quad (3)$$

where η corresponds to the detection efficiency of the APT analysis (η=0.62) and A to the interfacial area. In this sample, Γ_{Na} has been estimated at 0.9 at.nm^{-2}. This value is slightly below the averaged Gibbsian interfacial excess which was measured in CIGSe thin layers deposited on Mo rear contact (≈2 at.nm^{-2}) [43]. Besides, in sample A3, at grain boundary, Γ_{Na} has been estimated at 1.7 at.nm^{-2}. It seems to evidence that compared to Mo, the ITO rear contact may reduce the diffusion of Na originating from the SLG substrate, and that Na originating from PDT and DDT tend to segregate at the grain boundaries.

Discussion

The application of alkali treatments has been extensively investigated in the case of CIGSe based solar cells [11]. In this study, Na treatments have been performed on CIGSu absorber elaborated by the three stages process and grown on Mo and ITO rear contact. This allowed us to evidence the influence of Na PDT and DDT and the impact of Na on the local structural and optoelectronic properties of the CIGSu absorber.

Cathodoluminescence investigations have revealed the presence of defects in the CIGSu absorbers and their passivation due to the Na incorporation through PDT and DDT process. In the meantime, APT analysis reveals an In enrichment as well as a Cu depletion at the grain boundary in the sample A4. Such composition variations in the grain boundary may induced the formation of either V_{In} vacancies or Cu_{In} anti-site in the grain. This may lead to the observation of the defect energy band observed in CL spectrum of A4 around 1.45 eV, as seen on Figure 4.b. In fact, in the case of $CuInS_2$, it has been shown that V_{Cu} and Cu_{In} results in donor-acceptor transition around 1.43 eV and

1.39 eV, respectively [10]. Moreover, mass spectra evidenced the presence of Na inside the grain in sample A3 which underwent DDT and PDT (see Figure S4). Supplementary Na atoms introduced in the CIGSu layer may substitute to Cu atoms, leading to the formation of neutral point defect Na_{Cu} and to the passivation of the CIGSu grain interior. In addition, APT analysis also evidenced the planar segregation of Na at the grain boundary. This phenomenon has proven to reduce the atomic deficit or excess in CIGSe leading to improve the properties of the absorber [15,44]. Thus, the application of Na DDT and PDT seems to play an important role in the passivation of the grain interior as well as the grain boundaries (Figure 4.b). These Na PDT and DDT also proved to be responsible of the band grading in the CIGSu depth, highlighting the influence of Na incorporation on the band gap of the absorber. Indeed, this phenomenon has already been observed in CIGSe and is reported to arise from the interdiffusion between In and Ga atoms in the layer, triggered by the Na incorporation [40]. The band grading is also accompanied by the suppression of localized defects such as traps in the absorber limiting by the way the Shockley-Read-Hall recombination. It must be noted that in sample A4, where no variations are observed on the energy profile (Figure 7) and no In or Ga variations are observed along the depth of the APT volume. Finally, both phenomena, the band grading formation as well as the passivation of defects by Na PDT and DDT, showed to be independent of the nature of the rear contact.

Without Na PDT and DDT, differences can be highlighted between the use of Mo and ITO rear contact. Depending on the nature of the rear contact, the CL analysis in depth showed a different behaviour. In fact, the energy maps (Figure 6.d-6.f) as well as energy profiles (Figure 7) demonstrated the presence of a band grading toward the rear contact for the CIGSu grown on Mo contact, which is completely missing on ITO contact. Two hypotheses can be made to explain these observations. The first hypothesis concerns the diffusion of Na. In fact, as this was revealed by the APT analysis, Na can diffuse through the ITO rear contact. However, the amount of Na estimated at the grain boundary (0.9 at/nm²) seems to be slightly below the mean measured in the literature (2.0 at/nm²) in CIGSe grown on Mo back contact [10]. This may indicate that the diffusion coefficient of Na in Mo is higher than the one in ITO, inducing a lower amount of Na in sample A4 (ITO) than in A2 (Mo). As Na acts a role in the interdiffusion of In and Ga atoms during the growth of the CIGSu absorber [40], a lower amount of Na must reduce this effect leading to a decrease in the band grading effect. The second hypothesis concerns the CIGSu/ITO interface. In fact, concerning CIGSe based mono-junction grown on ITO rear contact, some studies have evidenced the formation of a Ga oxide (GaO_x) at the CIGSe/ITO interface [28]. As Ga only originates from the CIGSe, or in our case from the CIGSu layer, the formation of such GaO_x layer might deplete the amount of Ga contained in the absorber. This could lead to a decrease of the GGI, and so of the CIGSu bandgap. Moreover, the presence of GaO_x is also reported to slow down the Na diffusion from the SLG substrate [28]. Then, both of these mechanisms may interact together and lead to a complete absence of energy gradient along the depth of the CIGSu absorber grown on the ITO rear contact.

Finally, in this study, all three technics used for the structural and optical investigations have been also used to quantify the GGI. This estimation has been averaged on the entire sample using XRD and CL spectroscopy, and locally measured using APT analysis. Considering the small variations of the bandgap observed in the CIGSu absorber whatever their characteristics (less than 20 meV) (Figure 7), local measurement performed by APT can be consistently compared to CL or XRD for the GGI estimation. This shows that each technique is relevant for the measurement of the GGI even though the measurement is more or less localised from one technic to the other.

Conclusion

The present study investigated the influence of Na incorporation on pure sulphide CIGS absorber thin films for future applications in tandem solar cell. Four samples, featuring the CIGSu/(Mo or ITO)/SLG structures grown by a conventional three-stage process with and without Na incorporation, have been studied. It has been shown that the CIGSu layer was constituted of a single CIGSu phase whatever the rear contact. The analysis of the cathodoluminescence properties of the film revealed the presence of defects in samples without Na PDT and DDT. Moreover, Na incorporation through PDT and DDT proved to be crucial for defect passivation in CIGSu layer. The role of Na PDT and DDT in triggering the formation of a band gap grading, known to enhance PV cells properties, has been highlighted. Atom probe experiment revealed a segregation of Na at the grain boundaries in CIGSu grown on ITO,

which was not subjected to Na treatment. Thus, this clearly demonstrates that the use of ITO rear contact does not prevent the diffusion of Na from the substrate. Moreover, using ITO rear contact, it emerges that the amount of Na provided by the substrate is not sufficient to either passivate completely the layer nor favouring band gap grading. All three technics (XRD, CL and APT) have been used for the estimation of the GGI, and give consistent results. This work opens the doors for further investigations coupling those nano-scale analyses, notably to better understand the role of Na on the compositional distribution in the CIGSu layer. Further investigations will be particularly focused on the impact of Na on the grain boundaries chemistry.

CRediT authorship contribution statement

Richel Dongmo: Writing – Original Draft, Formal Analysis, Investigation, Validation, Visualization. **Rémi Demoulin:** Writing – Review & Editing, Formal analysis, Investigation, Conceptualization, Validation, Supervision, Project Administration. **Nicolas Barreau:** Writing – Review & Editing, Resources. **Léo Choubrac:** Resources. **Fabien Pineau:** Resources. **Etienne Talbot:** Writing – Review & Editing, Investigation, Formal Analysis, Conceptualization. **Sébastien Duguay:** Writing – Review & Editing, Visualization, Project Administration, Supervision, Funding Acquisition.

Declaration of competing interest

The authors declare that they have no known competing financial interests or personal relationships that could have appeared to influence the work reported in this paper.

Data availability

Data will be made available on request.

Acknowledgement

This work was supported by the Normandy Region and the CNRS Federation IRMA-FR 3095. The author acknowledges Fabien Cuvilly for his help in the acquisition of XRD pattern. APT data have been treated with the software GPM_3dSAT (IDDN.FR.001.430017.000.S.P.2020.000.10000).

References

[1] M. Di Sabatino, R. Hendawi, A.S. Garcia, Silicon Solar Cells: Trends, Manufacturing Challenges, and AI Perspectives, Crystals 14 (2024) 167. https://doi.org/10.3390/cryst14020167.

[2] J. Keller, K. Kiselman, O. Donzel-Gargand, N.M. Martin, M. Babucci, O. Lundberg, E. Wallin, L. Stolt, M. Edoff, High-concentration silver alloying and steep back-contact gallium grading enabling copper indium gallium selenide solar cell with 23.6% efficiency, Nat Energy 9 (2024) 467–478. https://doi.org/10.1038/s41560-024-01472-3.

[3] S. Rühle, Tabulated values of the Shockley–Queisser limit for single junction solar cells, Solar Energy 130 (2016) 139–147. https://doi.org/10.1016/j.solener.2016.02.015.

[4] J.F. Geisz, R.M. France, K.L. Schulte, M.A. Steiner, A.G. Norman, H.L. Guthrey, M.R. Young, T. Song, T. Moriarty, Six-junction III–V solar cells with 47.1% conversion efficiency under 143 Suns concentration, Nat Energy 5 (2020) 326–335. https://doi.org/10.1038/s41560-020-0598-5.

[5] S.P. Bremner, M.Y. Levy, C.B. Honsberg, Analysis of tandem solar cell efficiencies under AM1.5G spectrum using a rapid flux calculation method, Progress in Photovoltaics 16 (2008) 225–233. https://doi.org/10.1002/pip.799.

[6] H. Lin, M. Yang, X. Ru, G. Wang, S. Yin, F. Peng, C. Hong, M. Qu, J. Lu, L. Fang, C. Han, P. Procel, O. Isabella, P. Gao, Z. Li, X. Xu, Silicon heterojunction solar cells with up to 26.81% efficiency achieved by electrically optimized nanocrystalline-silicon hole contact layers, Nat Energy 8 (2023) 789–799. https://doi.org/10.1038/s41560-023-01255-2.

[7] N. Barreau, E. Bertin, A. Crossay, O. Durand, L. Arzel, S. Harel, T. Lepetit, L. Assmann, E. Gautron, D. Lincot, Investigation of co-evaporated polycrystalline Cu(In,Ga)S_2 thin film yielding 16.0 % efficiency solar cell, EPJ Photovolt. 13 (2022) 17. https://doi.org/10.1051/epjpv/2022014.
[8] H. Hiroi, Y. Iwata, S. Adachi, H. Sugimoto, A. Yamada, New World-Record Efficiency for Pure-Sulfide Cu(In,Ga)S_2 Thin-Film Solar Cell With Cd-Free Buffer Layer via KCN-Free Process, IEEE J. Photovoltaics 6 (2016) 760–763. https://doi.org/10.1109/JPHOTOV.2016.2537540.
[9] S. Merdes, R. Mainz, J. Klaer, A. Meeder, H. Rodriguez-Alvarez, H.W. Schock, M.Ch. Lux-Steiner, R. Klenk, 12.6% efficient CdS/Cu(In,Ga)S_2-based solar cell with an open circuit voltage of 879mV prepared by a rapid thermal process, Solar Energy Materials and Solar Cells 95 (2011) 864–869. https://doi.org/10.1016/j.solmat.2010.11.003.
[10] S. Siebentritt, A. Lomuscio, D. Adeleye, M. Sood, A. Dwivedi, Sulfide Chalcopyrite Solar Cells—Are They the Same as Selenides with a Wider Bandgap?, Physica Rapid Research Ltrs 16 (2022) 2200126. https://doi.org/10.1002/pssr.202200126.
[11] Y. Wang, S. Lv, Z. Li, Review on incorporation of alkali elements and their effects in Cu(In,Ga)Se_2 solar cells, Journal of Materials Science & Technology 96 (2022) 179–189. https://doi.org/10.1016/j.jmst.2020.07.050.
[12] C. Persson, A. Zunger, Anomalous Grain Boundary Physics in Polycrystalline $CuInSe_2$: The Existence of a Hole Barrier, Phys. Rev. Lett. 91 (2003) 266401. https://doi.org/10.1103/PhysRevLett.91.266401.
[13] F. Couzinie-Devy, E. Cadel, N. Barreau, L. Arzel, P. Pareige, Atom probe study of Cu-poor to Cu-rich transition during Cu(In,Ga)Se_2 growth, Applied Physics Letters 99 (2011) 232108. https://doi.org/10.1063/1.3665948.
[14] O. Cojocaru-Miredin, P.-P. Choi, D. Abou-Ras, D. Raabe, Characterization of CIGS grain boundaries using Atom Probe Tomography, in: 2011 37th IEEE Photovoltaic Specialists Conference, IEEE, Seattle, WA, USA, 2011: pp. 001965–001965. https://doi.org/10.1109/PVSC.2011.6186338.
[15] M. Raghuwanshi, E. Cadel, S. Duguay, L. Arzel, N. Barreau, P. Pareige, Influence of Na on grain boundary and properties of Cu(In,Ga)Se_2 solar cells, Progress in Photovoltaics 25 (2017) 367–375. https://doi.org/10.1002/pip.2869.
[16] D.J. Schroeder, A.A. Rockett, Electronic effects of sodium in epitaxial $CuIn_{1-x}Ga_xSe_2$, Journal of Applied Physics 82 (1997) 4982–4985. https://doi.org/10.1063/1.366365.
[17] D. Rudmann, D. Brémaud, A.F. Da Cunha, G. Bilger, A. Strohm, M. Kaelin, H. Zogg, A.N. Tiwari, Sodium incorporation strategies for CIGS growth at different temperatures, Thin Solid Films 480–481 (2005) 55–60. https://doi.org/10.1016/j.tsf.2004.11.071.
[18] L. Choubrac, E. Bertin, F. Pineau, L. Arzel, T. Lepetit, L. Assmann, T. Aloui, S. Harel, N. Barreau, On the role of sodium and copper off-stoichiometry in Cu (In,Ga)S_2 for photovoltaic applications: Insights from the investigation of more than 500 samples, Progress in Photovoltaics 31 (2023) 971–980. https://doi.org/10.1002/pip.3701.
[19] T. Schneider, C. Dethloff, T. Hölscher, H. Kempa, R. Scheer, Comparison of Mo and ITO back contacts in CIGSe solar cells: Vanishing of the main capacitance step, Progress in Photovoltaics 30 (2022) 191–202. https://doi.org/10.1002/pip.3476.
[20] Y.-S. Son, H. Yu, J.-K. Park, W.M. Kim, S.-Y. Ahn, W. Choi, D. Kim, J. Jeong, Control of Structural and Electrical Properties of Indium Tin Oxide (ITO)/Cu(In,Ga)Se_2 Interface for Transparent Back-Contact Applications, J. Phys. Chem. C 123 (2019) 1635–1644. https://doi.org/10.1021/acs.jpcc.8b11149.
[21] J. Keller, L. Stolt, O. Donzel-Gargand, T. Kubart, M. Edoff, Wide-Gap Chalcopyrite Solar Cells with Indium Oxide–Based Transparent Back Contacts, Solar RRL 6 (2022) 2200401. https://doi.org/10.1002/solr.202200401.
[22] A. Thomere, N. Barreau, N. Stephant, C. Guillot-Deudon, E. Gautron, M.T. Caldes, A. Lafond, Formation of Cu(In,Ga)S_2 chalcopyrite thin films following a 3-stage co-evaporation process, Solar Energy Materials and Solar Cells 237 (2022) 111563. https://doi.org/10.1016/j.solmat.2021.111563.
[23] B. Namnuan, S. Chatraphorn, Improving the photovoltaic performance of CIGS solar cells with the modified 3-stage co-evaporation process, Materials Science in Semiconductor Processing 179 (2024) 108485. https://doi.org/10.1016/j.mssp.2024.108485.
[24] K. Thompson, D. Lawrence, D.J. Larson, J.D. Olson, T.F. Kelly, B. Gorman, In situ site-specific specimen preparation for atom probe tomography, Ultramicroscopy 107 (2007) 131–139. https://doi.org/10.1016/j.ultramic.2006.06.008.

[25] P. Hovington, D. Drouin, R. Gauvin, CASINO: A new monte carlo code in C language for electron beam interaction —part I: Description of the program, Scanning 19 (1997) 1–14. https://doi.org/10.1002/sca.4950190101.
[26] D. Drouin, A.R. Couture, D. Joly, X. Tastet, V. Aimez, R. Gauvin, CASINO V2.42—A Fast and Easy-to-use Modeling Tool for Scanning Electron Microscopy and Microanalysis Users, Scanning 29 (2007) 92–101. https://doi.org/10.1002/sca.20000.
[27] K Kanaya, S Okayama, Penetration and energy-loss theory of electrons in solid targets, J. Phys. D: Appl. Phys. 5 (1972) 43–58. https://doi.org/10.1088/0022-3727/5/1/308.
[28] G. He, C. Yan, J. Li, X. Yuan, K. Sun, J. Huang, H. Sun, M. He, Y. Zhang, J.A. Stride, M.A. Green, X. Hao, 11.6% Efficient Pure Sulfide Cu(In,Ga)S_2 Solar Cell through a Cu-Deficient and KCN-Free Process, ACS Appl. Energy Mater. 3 (2020) 11974–11980. https://doi.org/10.1021/acsaem.0c02158.
[29] Y.-I. Kim, K.-B. Kim, M. Kim, Characterization of lattice parameters gradient of Cu($In_{1-x}Ga_x$)Se_2 absorbing layer in thin-film solar cell by glancing incidence X-ray diffraction technique, Journal of Materials Science & Technology 51 (2020) 193–201. https://doi.org/10.1016/j.jmst.2020.04.004.
[30] W. Li, X. Yan, A.G. Aberle, S. Venkataraj, Effect of sodium diffusion on the properties of CIGS solar absorbers prepared using elemental Se in a two-step process, Sci Rep 9 (2019) 2637. https://doi.org/10.1038/s41598-019-39283-2.
[31] S. Shukla, M. Sood, D. Adeleye, S. Peedle, G. Kusch, D. Dahliah, M. Melchiorre, G.-M. Rignanese, G. Hautier, R. Oliver, S. Siebentritt, Over 15% efficient wide-band-gap Cu(In,Ga)S_2 solar cell: Suppressing bulk and interface recombination through composition engineering, Joule 5 (2021) 1816–1831. https://doi.org/10.1016/j.joule.2021.05.004.
[32] C. Zhao, S. Yu, W. Tang, X. Yuan, H. Zhou, T. Qi, X. Zheng, D. Ning, M. Ma, J. Zhu, J. Zhang, C. Yang, W. Li, Advances in CIGS thin film solar cells with emphasis on the alkali element post-deposition treatment, Materials Reports: Energy 3 (2023) 100214. https://doi.org/10.1016/j.matre.2023.100214.
[33] W. Liu, H. Li, B. Qiao, S. Zhao, Z. Xu, D. Song, Highly efficient CIGS solar cells based on a new CIGS bandgap gradient design characterized by numerical simulation, Solar Energy 233 (2022) 337–344. https://doi.org/10.1016/j.solener.2022.01.054.
[34] L. Thirumalaisamy, N. Ahsan, K. Sivaperuman, M. Kim, S. Kunjithapatham, Y. Okada, Engineering of sub-band in $CuGaS_2$ thin films via Mo doping by chemical spray pyrolysis route, Thin Solid Films 709 (2020) 138252. https://doi.org/10.1016/j.tsf.2020.138252.
[35] S. Siebentritt, M. Igalson, C. Persson, S. Lany, The electronic structure of chalcopyrites—bands, point defects and grain boundaries, Progress in Photovoltaics 18 (2010) 390–410. https://doi.org/10.1002/pip.936.
[36] S.-H. Wei, A. Zunger, Band offsets and optical bowings of chalcopyrites and Zn-based II-VI alloys, Journal of Applied Physics 78 (1995) 3846–3856. https://doi.org/10.1063/1.359901.
[37] H. Hiroi, Y. Iwata, K. Horiguchi, S. Adachi, N. Sakai, H. Sugimoto, 960mV open circuit voltage chalcopyrite solar cell, in: 2015 IEEE 42nd Photovoltaic Specialist Conference (PVSC), IEEE, New Orleans, LA, 2015: pp. 1–4. https://doi.org/10.1109/PVSC.2015.7355655.
[38] O. Lundberg, M. Edoff, L. Stolt, The effect of Ga-grading in CIGS thin film solar cells, Thin Solid Films 480–481 (2005) 520–525. https://doi.org/10.1016/j.tsf.2004.11.080.
[39] J. Zhang, Z. Ma, Y. Zhang, X. Liu, R. Li, Q. Lin, G. Fang, X. Zheng, W. Li, C. Yang, J. Li, J. Gong, X. Xiao, Highly efficient narrow bandgap Cu(In,Ga)Se_2 solar cells with enhanced open circuit voltage for tandem application, Nat Commun 15 (2024) 10365. https://doi.org/10.1038/s41467-024-54818-6.
[40] E.S. Mungan, X. Wang, M.A. Alam, Modeling the Effects of Na Incorporation on CIGS Solar Cells, IEEE J. Photovoltaics 3 (2013) 451–456. https://doi.org/10.1109/JPHOTOV.2012.2221082.
[41] D. Abou-Ras, B. Marsen, T. Rissom, F. Frost, H. Schulz, F. Bauer, V. Efimova, V. Hoffmann, A. Eicke, Enhancements in specimen preparation of Cu(In,Ga)$(S,Se)_2$ thin films, Micron 43 (2012) 470–474. https://doi.org/10.1016/j.micron.2011.11.004.
[42] N. Mavrikakis, W. Saikaly, D. Mangelinck, M. Dumont, Segregation of Sn on migrating interfaces of ferrite recrystallisation: quantification through APT measurements and comparison with the solute drag theory, Materialia 9 (2020) 100541. https://doi.org/10.1016/j.mtla.2019.100541.

[43] O. Cojocaru-Mirédin, M. Raghuwanshi, R. Wuerz, S. Sadewasser, Grain Boundaries in Cu(In, Ga)Se_2 : A Review of Composition–Electronic Property Relationships by Atom Probe Tomography and Correlative Microscopy, Adv Funct Materials 31 (2021) 2103119. https://doi.org/10.1002/adfm.202103119.
[44] X. Sun, F. Jiang, J. Feng, Roles of sodium induced defects in CuInSe2 by first principles calculation, Computational Materials Science 47 (2009) 31–34. https://doi.org/10.1016/j.commatsci.2009.06.012.